Biochemical Characterization of Recombinant Hepatitis C Virus Nonstructural Protein 4B: Evidence for ATP/GTP Hydrolysis and Adenylate Kinase Activity[†]

Aaron A. Thompson, Aihua Zou, Jiangli Yan, Rohit Duggal, Weidong Hao, David Molina,[‡] Ciarán N. Cronin, and Peter A. Wells*

Department of Biochemical Pharmacology, La Jolla Laboratories, Pfizer Global Research and Development Inc., San Diego, California 92121

Received September 12, 2008; Revised Manuscript Received December 17, 2008

ABSTRACT: While nonstructural protein 4B (NS4B) from hepatitis C virus (HCV) is absolutely required for viral propagation, a full understanding of the enzymatic properties of this protein is lacking. Previous studies suggest that NS4B is located at the endoplasmic reticulum and that the protein structure consists of four central transmembrane domains with the N- and C-termini located in the cytoplasm of the host cell. To characterize the enzymatic activity of NS4B, the full-length protein with a C-terminal His tag was expressed in *Sf9* insect cells and stabilized with nonionic detergents during purification. Chemical cross-linking experiments using GTP-γ-azidoanilide and ATP-γ-azidoanilide and equilibrium binding analyses with GTPγS and ATPγS show that both GTP and ATP are bound by NS4B, with ATP displaying a higher affinity. Analyses of enzymatic reactions catalyzed by NS4B indicate that the terminal phosphate groups of ATP, GTP, and GDP are removed to produce ADP, GDP, and GMP, respectively. The k_{cat} for hydrolysis of GTP by purified NS4B compared favorably with the k_{cat} for hydrolysis of GTP by Ras-p21 in the absence of GTPase activating proteins (GAPs). In addition to the hydrolysis of NTP and NDP substrates, adenylate kinase activity was detected in purified preparations of NS4B with the reverse reaction 2ADP → ATP + ADP, yielding a larger k_{cat} compared to that of the forward reaction ATP + AMP → 2ADP. These studies suggest that HCV NS4B possesses both adenylate kinase activity and nucleotide hydrolase activity. Mutation of amino acids in the Walker A and B motifs of NS4B resulted in decreased affinity for both GTPγS and ATPγS as well as decreased ATP hydrolysis and AK activity.

Hepatitis C virus (HCV), a member of the Flaviviridae family, contains a single-stranded positive-sense RNA genome of approximately 9600 nucleotides. Like other members of this family of viruses, translation of a single open reading frame yields a large polyprotein that is proteolytically processed by both viral and cellular proteases, resulting in at least 10 different mature proteins which are required for viral propagation. Following translation, all of the nonstructural proteins and the viral RNA colocalize to a dense perinuclear matrix termed the "membranous web" that is believed to be derived from endoplasmic reticulum (ER) (*1*−*5*). These altered membranes are thought to serve as a scaffold for the replication process, and this compartmentalization has been proposed to protect the replication complex from antiviral defense mechanisms of the host cell (*6, 7*). In this sequestered environment, HCV RNA is protected from nuclease degradation (*6, 8*−*10*) and viral replicase activity is shielded from proteolytic degradation (*6, 9*). Although the mechanism is unclear, it has been shown that the NS4B[1] protein alone is sufficient to induce formation of the membranous web in U-2 OS cells (*2*).

NS4B is a relatively hydrophobic 27 kDa protein with four proposed transmembrane (TM) domains that are centrally located on the basis of hydrophobicity plots and glycosylation studies (*11*). There is also a report that cysteines located at the very C-terminus are palmitoylated, which would tether this end of the protein to the membrane (*12*). Several different topology models exist for the N-terminal portion of the protein proposing the existence of a fifth TM domain (TM X, residues 60−80) whose orientation is influenced by the NS5A protein (*13*), an amphipathic helix in the first 29 amino acids (*14*), and/or a basic leucine zipper between residues ~20 and 55 which could be involved in protein−protein interactions (*15*). In the context of the replication complex, all of the other nonstructural proteins are believed to interact with NS4B in some manner (*3, 16*−*18*), including interactions with itself (*12, 16*). The NS4B protein of HCV and related viruses within the Flaviviridae family are also known

[†] This work was supported by the Pfizer Global Research and Development La Jolla Postdoctoral Program.

* To whom correspondence should be addressed. E-mail: peter.a.wells@pfizer.com. Telephone: (858) 638-3856. Fax: (858) 622-3239.

[‡] Present address: Sapphire Energy, 3115 Merryfield Row, San Diego, CA 92121.

[1] Abbreviations: AK, adenylate kinase (EC 2.7.4.3); ATPγAA, ATP-γ-azidoanilide; ATPγS, adenosine 5′-(γ-thio)triphosphate; GTPγAA, GTP-γ-azidoanilide; GTPγS, guanosine 5′-(γ-thio)triphosphate; NS4B, nonstructural protein 4B from hepatitis C virus-1b Con1 isolate; NS4B-2M, K135E/D228N NS4B double mutant; NS4B-5M, I131N/G132A/K135E/F211A/D228N NS4B quintuple mutant; MOI, multiplicity of infection; CD, circular dichroism; LC−MS, liquid chromatography and mass spectroscopy.

10.1021/bi801747p CCC: $40.75
Published on Web 01/15/2009

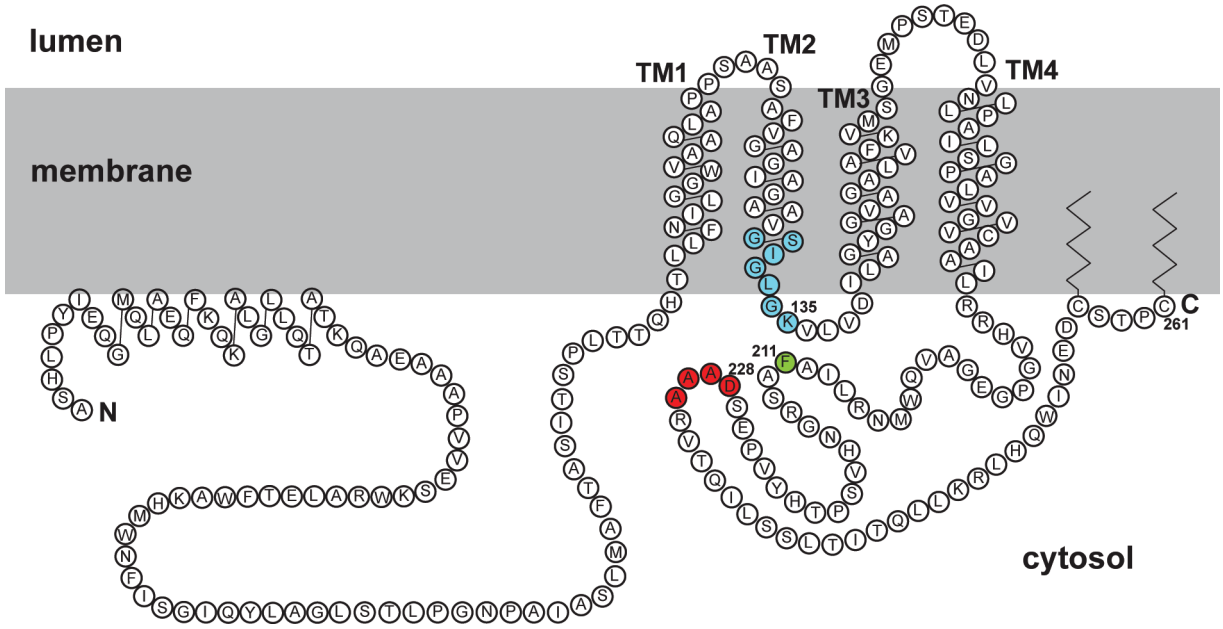

FIGURE 1: Diagram of the proposed HCV NS4B topology within the lipid bilayer. The NS4B genotype 1b amino acid sequence topology is depicted with four putative transmembrane domains as defined by the work of Persson and colleagues (*11*). The boundaries of the putative N-terminal amphipathic helix are as described by Elazar et al. (*14*). The C-terminal Cys residues at positions 257 and 261 are palmitoylated as described by Yu et al. (*12*). Nucleotide binding motifs A, B, and G are colored blue, red, and green, respectively. While the three-dimensional structure of the cytosolic domains is unknown, biochemical data suggest nucleotide binding motifs A, B, and G are near each other in the folded protein.

to be required in the *cis* configuration since *trans* complementation is unable to restore viral infectivity (*1, 19*−*21*). Recently, a nucleotide binding motif was identified on NS4B near the postulated cytosolic−protein interface between TM domains 2 and 3 (Walker A motif) and a central portion of the C-terminus (Walker B motif) (Figure 1) (*22*). This nucleotide binding motif has been implicated in the binding and hydrolysis of GTP (*22*) and ATP (*23, 24*). The finding of adaptive mutations (K135T and R232S) within the nucleotide binding motifs of NS4B permitting HCV replication in cell culture (*25, 26*) underscores the need for further study of NS4B enzymatic activity.

Purification and biochemical characterization of NS4B are technically difficult due to the hydrophobic properties of this integral membrane protein. To improve our understanding of the enzymatic activity of NS4B, recombinant protein with a C-terminal six-histidine tag was expressed in a baculovirus *Sf9* cell system, solubilized using nonionic detergents, and purified using nickel affinity chromatography. Biochemical studies with this purified protein were undertaken to determine substrate specificity and rates of hydrolysis for phosphonucleotides. Binding studies using purified NS4B indicated that phosphonucleotides containing the adenine base demonstrated greater affinity for the protein than those containing the guanine base. Measurements of the kinetic parameters of reactions catalyzed by NS4B reveal a relatively slow hydrolysis of ATP and GTP to the respective NDP, and a more rapid conversion of GDP to GMP. Furthermore, reaction mixtures containing only ADP and NS4B resulted in the formation of both AMP and ATP, indicating adenylate kinase activity (EC 2.7.4.3). These findings and their potential relevance to the role of NS4B are discussed.

EXPERIMENTAL PROCEDURES

NS4B Cloning and Expression. The HCV-1b Con1 NS4B gene, bases 5475−6257 from GenBank entry AJ238799, was amplified by PCR using KOD DNA polymerase and the amplified fragment blunt-end cloned into a custom-designed TOPO-adapted derivative of pFastBac1 (Invitrogen). This customization appends the C-terminus of the amplified sequence with QGENLYFQGHHHHHH that contains a polyhistidine purification tag preceded by a TEV protease cleavage site. An ATG translation initiation codon was encoded by the 5′ amplification primer. Point mutations were introduced by using a QuikChange kit (Stratagene) and verified by DNA sequencing. Recombinant baculoviruses were generated by using the Bac-to-Bac system (Invitrogen) and were used to infect *Sf*9 insect cells at a density of 2×10^6 cells/mL at a MOI of 5. The infected cells were allowed to continue to grow for 48 h prior to being harvested. The cell pellets were stored frozen at −80 °C.

NS4B Purification. Frozen cell pellets were thawed, resuspended in TBS [50 mM Tris (pH 8.0) and 150 mM NaCl] and sonicated. The suspension was centrifuged at 34000*g* for 30 min and the membrane pellet resuspended in TBS. The cell membrane fraction was washed twice more with TBS by resuspension and centrifugation as described above prior to extraction. Following the third wash with TBS, the membrane fraction was resuspended in 50 mM Tris (pH 8.0), 400 mM NaCl, 0.1% (w/v) *n*-octyl β-D-glucopyranoside (BOG, Anatrace), 0.1% (w/v) *n*-dodecyl β-D-maltopyranoside (DDM, Anatrace), 10 mM imidazole (pH 8.0), 10% glycerol, Roche "Complete-EDTA" protease inhibitor cocktail tablets (1 tablet/50 mL), and 4 mM 2-mercaptoethanol. The membrane fraction was extracted overnight in this buffer with stirring at 4 °C. Following extraction, the suspension was centrifuged at 35000*g* for 30 min and the supernatant fraction subjected to batch absorption with Ni-NTA (Qiagen) affinity resin at 4 °C with mixing for 1 h. The slurry was poured into a column and washed with extraction buffer containing

20 mM imidazole (pH 8.0). NS4B protein was eluted with extraction buffer containing 500 mM imidazole (pH 8.0). Following elution, the protein was dialyzed against 50 mM HEPES (pH 7.0), 400 mM NaCl, 10% (v/v) glycerol, 0.05% (w/v) BOG, 0.05% (w/v) DDM, and 2 mM DTT for 16 h at 4 °C and frozen on dry ice.

SDS−PAGE and Western Immunoblots. Proteins were separated on 4 to 12% acrylamide gels and stained with either Coomassie Blue (Simply Blue Invitrogen) or SYPRO-Orange (Invitrogen). For Western blots, proteins were transferred from SDS−PAGE gels to PVDF membranes and probed with a monoclonal antibody targeting a linear epitope located at the NS4B N-terminus (catalog no. C8A246M, Meridian Life Sciences, Inc.). Digitized images were obtained following chromogenic detection.

LC−MS Analysis. All LC−MS analyses were performed using a Waters LCT Premier mass spectrometer (Micromass Technologies Ltd.) in ES+ ion mode coupled to a Waters 1525 μ Binary HPLC Pump system equipped with a Waters 2777C Sample Manager. The LC separation was performed on a C4 MicroTrap Protein column (Michrom Biosciences Inc.; 1 mm × 8 mm) with an isocratic gradient of 85% solvent A (99.8% acetonitrile and 0.2% formic acid) and 15% solvent B (99.8% water and 0.2% formic acid), and the data were analyzed and deconvoluted with MassLynx version 4.0 (Micromass Ltd.).

CD Spectroscopy. All CD spectra were recorded on a Jasco model J-715 circular dichroism spectrometer at ambient room temperature. Wavelength data are the average of three scans from 250 to 190 nm in 1 nm steps and are subtracted from buffer controls. A 0.02 cm path length cell containing 35 μL of 29 μM protein was used in all CD experiments.

NTPγAA UV Cross-Linking Studies. Cross-linking was performed in 20 μL reaction mixtures consisting of 1.5 μg of NS4B, 150 mM NaCl, 50 mM HEPES (pH 7.0), 5 mM $MgCl_2$, ~0.004% (w/v) DDM, ~0.004% (w/v) BOG, 0.75% (v/v) glycerol, and either ^{32}P-labeled ATP-γ-azidoanilide or GTP-γ-azidoanilide at 10 μM ([γ-^{32}P]ATPγAA, 9.6 Ci/mmol; [γ-^{32}P]GTPγAA, 44.0 Ci/mmol; Affinity Labeling Technologies Inc.). The reaction mixtures were incubated on ice for 1 h in the presence or absence of nonhydrolyzable adenosine 5′-(γ-thio)triphosphate or guanosine 5′-(γ-thio)triphosphate (ATPγS or GTPγS; Sigma). The reaction mixtures were then placed in a siliconized glass nine-well plate (Hampton Research) on ice and exposed to 254 nm UV light (Spectroline model EF-160C) for 2 min at a distance of 3 cm. Un-cross-linked photoreactive NTPγAAs were quenched by addition of 1 μL of 1 M DTT and exposed to the UV light for an additional 2 min. Samples of labeled proteins were loaded onto a 4 to 12% acrylamide SDS−NuPAGE gel (Invitrogen), stained with SYPRO-Orange (Invitrogen) following electrophoresis, analyzed with a fluorescence scanner (Storm840, Molecular Dynamics), dried, and finally visualized by PhosphorImager analysis (Storm840, Molecular Dynamics). Images were processed using ImageQuant (Molecular Dynamics) with no visual adjustments (brightness, contrast, or gamma). Samples for LC−MS analysis were similar except that the reaction mixtures contained 100 μM nonradiolabeled ATPγAA or GTPγAA and were exposed to 254 nm UV light for only 15 s before and after the reactions had been quenched with 1 μL of 1 M DTT.

NTPγS Binding Assays. Binding was analyzed with 100 μL reaction mixtures containing ~1.5 μg of purified NS4B, 150 mM NaCl, 50 mM HEPES (pH 7.0), 5 mM $MgCl_2$, 2% (v/v) glycerol, 0.01% (w/v) DDM, 0.01% (w/v) BOG, 2 mM DTT, and either adenosine 5′-[γ-^{35}S]triphosphate or guanosine 5′-[γ-^{35}S]triphosphate ([γ-^{35}S]ATPγS or [γ-^{35}S]-GTPγS, 1250 Ci/mmol; Perkin-Elmer) in a 96-well microtiter plate. The plate was placed on a 30 °C heating block for a 2 h equilibration for K_d experiments, variable times for k_{off}/k_{on} experiments, or for 1 h for competition experiments. Following the incubation, protein−ligand complexes were transferred to 96-well Immobilon P microfiltration plates (Millipore catalog no. MAIPN0B50) and filtered using a Millipore Multiscreen vacuum manifold. Before filtration, the plates were prewet with 70% ethanol, washed with buffer [150 mM NaCl and 50 mM HEPES (pH 7.0)] supplemented with 50 μM GTP (Sigma), and then washed with the same buffer without GTP. After addition of the reaction mixture, the filters were extensively washed with buffer and allowed to dry, and 100 μL of Microscint 20 (Perkin-Elmer) was added before the samples were counted in a Packard TopCount NXT counter (Perkin-Elmer). Equilibrium dissociation constants were determined by fitting the data to a one-site binding hyperbola using GraphPad Prism version 5.0. Experimental rate constants, k_{obs}, were determined by fitting kinetic data to the first-order rate equation. IC_{50} values for competing nucleotides were determined by fitting dose−response data to the four-parameter logistic equation, and the IC_{50} values were converted to K_i values (inhibition constant) using the Cheng−Prusoff equation (*27*) and assuming a fully reversible competitive mechanism.

HPLC Analysis of Substrate Hydrolysis. NS4B reaction mixtures were applied to a reversed-phase Tosoh TSK-GEL ODS-100V C_{18} column (2.0 mm × 15 cm) using an Agilent model 1100 HPLC system with an isocratic mobile phase containing either 97% 20 mM *tert*-butylamine (pH 6.75 with H_3PO_4), 2.7% acetonitrile, and 0.3% methanol when testing adenosine nucleotides (λ = 259 nm) or 98% 20 mM *tert*-butylamine (pH 6.75 with H_3PO_4), 1.8% acetonitrile, and 0.2% methanol when testing guanosine nucleotides (λ = 253 nm). All absorbance peaks were identified by comparison with the retention times of standards and quantitated by integration of peak areas. Reaction mixtures contained nucleotide substrate and 450 nM active NS4B in 50 mM HEPES (pH 7.0), 150 mM NaCl, 5 mM $MgCl_2$, 2% glycerol, and 2 mM DTT. For determination of enzyme kinetic parameters, reaction mixtures containing adenosine nucleotides were incubated for 120 min at room temperature and guanosine nucleotides were incubated for 150 min at room temperature before the reactions were quenched with EDTA. The reaction velocities were plotted as a function of [S] and fit to the Michaelis−Menten equation to determine K_m and V_{max} values. The turnover rate (k_{cat}) was calculated as $k_{cat} = V_{max}/E_0$, where E_0 is the active NS4B concentration determined from the maximum amount of [γ-^{35}S]ATP bound and assuming an ATPγS:NS4B stoichiometry of 1:1 (supported by a Hill slope of 1 in binding experiments). For the analysis of reaction mixtures using [2,8-^{3}H]ADP (Amersham, catalog no. NET-241) as a substrate for NS4B, the same Tosoh TSK-GEL ODS-100V C_{18} column was installed on an Agilent model 1100 HPLC system equipped with a radiometric detector (β-RAM model 3, IN/US Systems, Inc.).

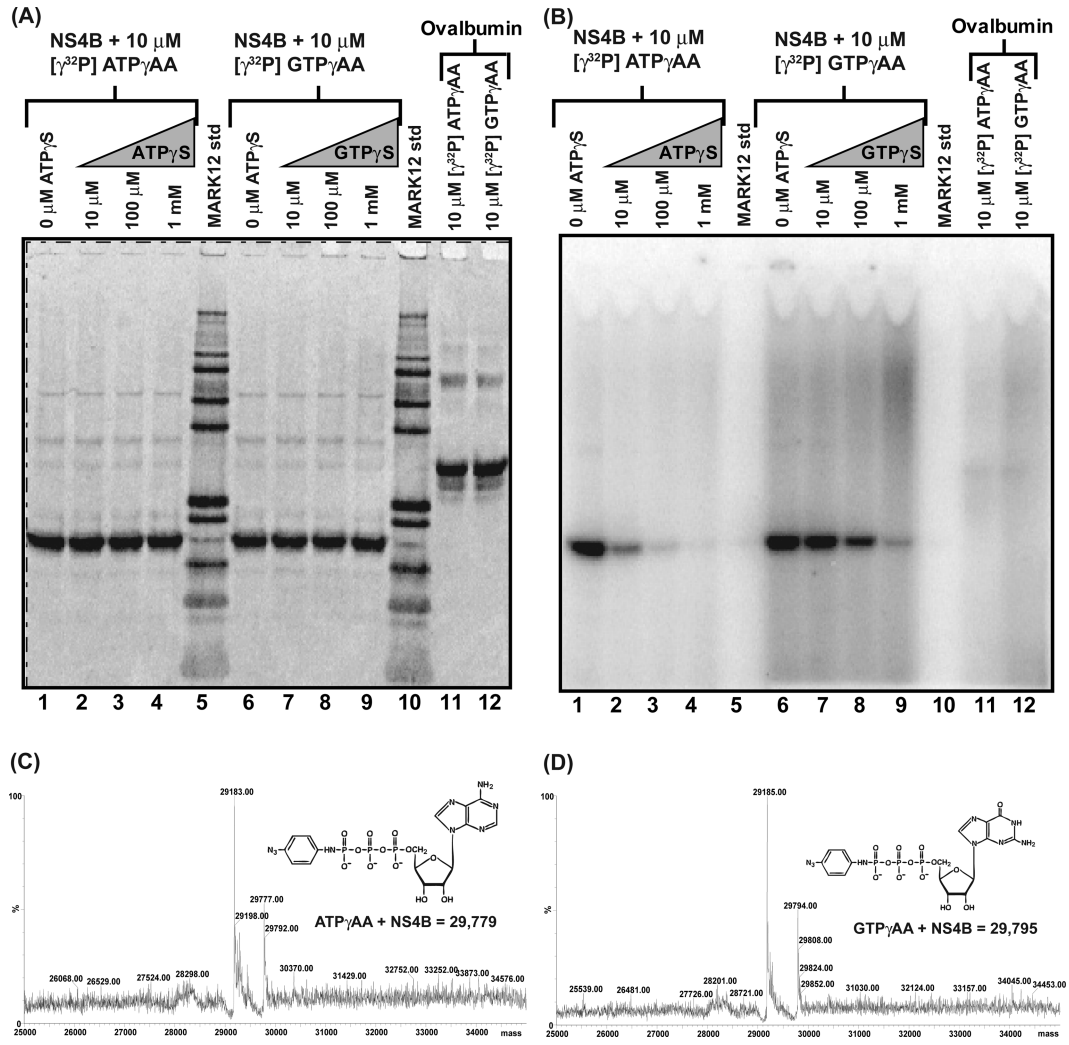

FIGURE 2: ATPγAA/GTPγAA-NS4B cross-linking. (A) SYPRO-Orange protein-stained SDS−PAGE gel showing purified NS4B (and ovalbumin) after UV cross-linking with [γ-^{32}P]NTPγAAs. (B) Phosphorimage of the same SDS−PAGE gel from panel A indicating [γ-^{32}P]NTPγAA cross-linking to 29 kDa NS4B. The addition of increasing amounts of ATPγS or GTPγS to the reaction mixture reduces the level of labeling of the 29 kDa band with [γ-^{32}P]ATPγAA and [γ-^{32}P]GTPγAA. (C) LC−MS of UV cross-linked NS4B−ATPγAA complex with an observed mass of 29777 Da (expected mass of the NS4B−ATPγAA complex of 29779 Da). (D) LC−MS of the UV-cross-linked NS4B−GTPγAA complex with an observed mass of 29794 Da (expected mass of the NS4B−GTPγAA complex of 29795 Da).

RESULTS

Western Immunoblot, LC−MS, and Circular Dichroism of NS4B. The NS4B construct used for these studies contained a six-histidine purification tag at the C-terminus preceded by a short TEV protease cleavage sequence. The recombinant NS4B protein was expressed in *Sf9* insect cells using a baculovirus vector. Membrane proteins were extracted from cell pellets using nonionic detergents, and NS4B was purified by Ni-IMAC chromatography. Western immunoblots using a monoclonal antibody directed against the N-terminus of NS4B indicated that the major 29 kDa band in the Ni-IMAC eluate was NS4B (Figure 1A of the Supporting Information). LC−MS analysis of the purified protein yielded a mass of 29184 Da which is consistent with the loss of the N-terminal methionine and a single acetylation (Figure 1B of the Supporting Information). While limited tryptic digestion combined with MS/MS amino acid sequencing confirmed the presence of NS4B, attempts at N-terminal sequencing of the purified protein were unsuccessful, indicating that the N-terminus was blocked (data not shown). To evaluate the effects of the detergent extraction and purification procedure on protein conformation, the secondary structure of the purified NS4B was examined by CD. The far-ultraviolet circular dichroism spectrum of the purified protein displayed negative minima at 209 and 222 nm and a maximum at 193 nm (Figure 1C of the Supporting Information). These features in the CD spectrum indicated the purified protein possesses a high content of α-helix and that the detergent extraction and purification process yielded NS4B protein with a well-folded secondary structure.

NS4B Binds both GTP and ATP. Recombinant NS4B protein was incubated with photoreactive [γ-^{32}P]GTPγAA and [γ-^{32}P]ATPγAA NTP analogues and UV-irradiated to cross-link bound NTPγAA to the protein. SDS−PAGE with visualization of ^{32}P-labeled protein demonstrated binding of both [γ-^{32}P]GTPγAA and [γ-^{32}P]ATPγAA to the 29 kDa NS4B protein (Figure 2A,B, lanes 1 and 6). This binding was specific for the NS4B protein as there was no labeling of minor contaminating protein bands in the NS4B preparation or of a control protein (ovalbumin) (Figure 2B, lanes 11 and 12). The specificity of the labeling was further

Table 1: NS4B Binding Constants for ATPγS and GTPγS

	NS4B construct	ATPγS	GTPγS
saturation−equilibrium K_d with Mg^{2+}	wild type (WT)	4.1 ± 0.6 μM	42 ± 2 μM
saturation−equilibrium K_d with Mn^{2+}	WT	0.115 ± 0.005 μM	1.3 ± 0.2 μM
k_{on} with Mg^{2+}	WT	43 ± 5 M^{-1} s^{-1}	9 ± 1 M^{-1} s^{-1}
k_{off} with Mg^{2+}	WT	(240 ± 40) × 10^{-6} s^{-1}	(130 ± 9) × 10^{-6} s^{-1}
kinetic K_d with Mg^{2+} (k_{off}/k_{on})	WT	5.6 ± 1.1 μM	15 ± 2 μM
saturation−equilibrium K_d (Mg^{2+})	NS4B-2M	67 ± 12 μM	259 ± 61 μM
saturation−equilibrium K_d (Mg^{2+})	NS4B-5M	no binding	~7 mM

demonstrated by competition experiments using cold guanosine 5′-(γ-thio)triphosphate or cold adenosine 5′-(γ-thio)triphosphate. Increasing the concentration of these competitors resulted in a concomitant decrease in the magnitude of the radiolabel signal from the NS4B band (Figure 2B, lanes 2−4 and 7−9). Cross-linking with [α-^{32}P]8N_3-ATP, an analogue that energetically favors the syn conformation due to the presence of the azide moiety at the purine ring C8 position, was unsuccessful (data not shown).

To determine the number of NTPγAA analogues bound per molecule of NS4B protein, the masses of the NS4B−NTPγAA complexes were examined using LC−MS. In these experiments, cross-linking of GTPγAA and ATPγAA to the protein is expected to result in increases in mass of 611.3 and 595.3 Da for GTPγAA and ATPγAA, respectively. The expected mass of a NS4B−GTPγAA complex is 29795 Da, matching the observed 29794 Da peak, whereas the expected mass of a NS4B−ATPγAA complex is 29779 Da, with a 29777 Da LC−MS peak observed (Figure 2C,D). Peaks correlating with cross-linking of multiple NTPγAAs to NS4B were not observed, indicating a 1:1 stoichiometry of NTP binding to NS4B.

Dissociation Constants (K_d) of GTPγS versus ATPγS. To compare NS4B binding affinities for nonhydrolyzable GTP and ATP analogues, a filter-based assay was used to measure the saturation−equilibrium dissociation constants (K_d) for [γ-^{35}S]GTP and [γ-^{35}S]ATP at physiological NaCl concentrations. Maximal binding of GTPγS and ATPγS was observed at pH 7.0 after incubation for 2 h at 30 °C (data not shown). Numerous divalent metal ions, including Ca^{2+}, Co^{2+}, Mg^{2+}, Mn^{2+}, Ni^{2+}, and Zn^{2+} (chloride salts), were tested with only Mg^{2+} and Mn^{2+} resulting in significant NTPγS binding. Both radiolabeled ligands, [γ-^{35}S]GTP and [γ-^{35}S]ATP, exhibited greater binding affinity for NS4B in the presence of Mn^{2+} compared to Mg^{2+} by approximately 30-fold (Table 1). Furthermore, the measurement of equilibrium dissociation constants (K_d) for these NTP analogues demonstrated that NS4B bound [γ-^{35}S]ATP with greater affinity than [γ-^{35}S]GTP by a factor of ~10 in the presence of either Mg^{2+} or Mn^{2+} (Table 1 and Figure 3A,3B). To further define the affinity of NS4B for divalent metal ions, the equilibrium dissociation constants for Mg^{2+} and Mn^{2+} were determined in the presence of excess [γ-^{35}S]ATP. The K_d for Mg^{2+} was 277 μM, and the K_d for Mn^{2+} was 19 μM. Using published values for the free intracellular concentrations of Mg^{2+} (~500 μM) and Mn^{2+} (~0.5 μM) (*28, 29*), the fractional occupancies of NS4B in the cell were calculated as 64% saturated with Mg^{2+} and 2.6% saturated with Mn^{2+}, suggesting that Mg^{2+} is the cation used by NS4B *in vivo*. However, if Mn^{2+} is sequestered in the specialized endoplasmic reticulum within the cell where HCV replicates, Mn^{2+} would be bound by NS4B, and this would result in tighter binding of ATP or GTP.

In addition to determining the equilibrium dissociation constants (K_d) for [γ-^{35}S]ATP and [γ-^{35}S]GTP, the experimental rate constants (k_{obs}) for binding were determined kinetically at various ligand concentrations in the presence of Mg^{2+} (Figure 2A,B of the Supporting Information). Linear plots of k_{obs} versus ligand concentration were used to determine the on rate (k_{on}) and the off rate (k_{off}) (Figure 4A,B). The k_{on} for [γ-^{35}S]ATP was approximately 5 times greater than the k_{on} observed for [γ-^{35}S]GTP (Table 1); however, the k_{off} for GTPγS was approximately half of that determined for ATPγS, which translates to half-lives of 90 and 48 min for GTPγS and ATPγS, respectively. The K_d values determined from k_{on} and k_{off} in the presence of Mg^{2+} were comparable to the K_d values determined by the equilibrium binding studies.

Mutations within the Nucleotide Binding Motif Impair Binding of NTP to NS4B. To confirm that ATP and GTP binding is mediated by the NS4B nucleotide binding motif, two mutant proteins were engineered with amino acid substitutions in the Walker sequences. The selection of these mutations was based on previous studies of p21-Ras and HCV NS4B (*30, 31*). A double mutant (NS4B-2M) was created in which Lys135 from Walker motif A (PM1) was mutated to a glutamic acid, thereby switching the charge, and Asp228 from Walker motif B (PM2) was mutated to an Asn to preserve steric bulk. In addition to this double mutant, a quintuple mutant (NS4B-5M) containing three additional

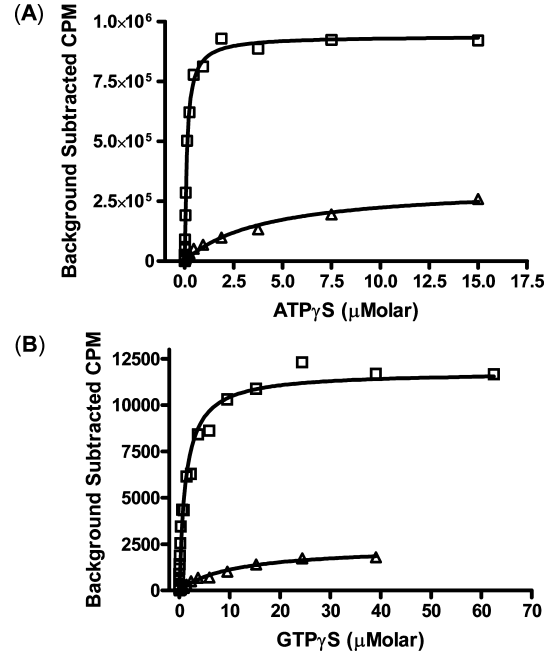

FIGURE 3: Saturation−equilibrium determination of NS4B−ATPγS and −GTPγS disassociation constants. Saturation−equilibrium Langmuir isotherm of NS4B binding to various concentrations of (A) [γ-^{35}S]ATP or (B) [γ-^{35}S]GTP with either 5 mM $MnCl_2$ (□) or 5 mM $MgCl_2$ present (△).

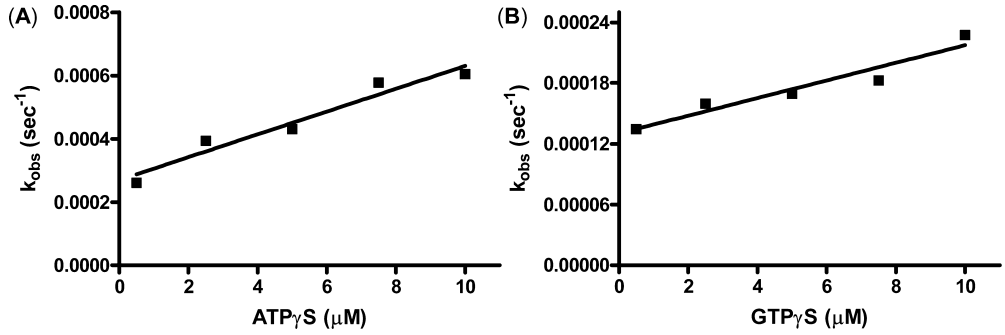

FIGURE 4: Kinetic determination of NS4B−ATPγS and −GTPγS dissociation constants. (A) Plot showing k_{obs} values for ATPγS and (B) GTPγS as a function of ligand concentration. The k_{on} and k_{off} rate constants were determined from the slope and *Y*-intercept, respectively, of a linear fit to the data. The kinetic data used to obtain the k_{obs} values are provided as Supporting Information.

Table 2: IC_{50} and K_i Values for Adenosine and Guanine Substrates in HCV NS4B−ATPγS Binding Assay

ligand	IC_{50} (μM)	K_i (μM)
ATP	1.44	0.50
3′-dATP	1.77	0.62
dATP	2.46	0.86
ADP	187.9	65.4
AMP	700.1	243.5
GTP	102.8	35.8
GDP	4674	1626
GMP	>13000	4581
ATPγS	10.08	3.51
ATPβγN	100.2	34.9
GTPγS	267	93
cAMP	525	183
cGMP	>8900	>3000

mutations, Ile131 to Asn (Walker motif A PM1), Gly132 to Ala (Walker motif A PM1), and Phe211 to Ala (G motif), was generated. These mutant NS4B proteins were expressed in the same *Sf*9 cell line and purified in the same manner as WT NS4B. SDS−PAGE analysis indicated the protein purity was equivalent for WT NS4B and the mutant protein preparations (Figure 3 of the Supporting Information). The two mutant NS4B proteins were tested for their ability to bind [γ-^{35}S]ATP and [γ-^{35}S]GTP in the equilibrium binding assay. Compared to WT NS4B, the NS4B-2 M mutant displayed a 16-fold increase in the K_d for [γ-^{35}S]ATP and a 6-fold increase in the K_d for [γ-^{35}S]GTP (Table 1). The quintuple mutant, NS4B-5M, showed no measurable binding of either [γ-^{35}S]ATP or [γ-^{35}S]GTP at concentrations of up to 0.5 mM.

Competition with NTP Analogues. To explore the possibility that NS4B may preferentially bind substrates other than purine triphosphates, binding assays using WT NS4B and [γ-^{35}S]ATP (7.5 μM) were performed in the presence of competing nucleotides at concentrations of 1 and 10 μM (Figure 4 of the Supporting Information). These results indicated higher affinity of NS4B for adenine nucleotides over all other nucleotides. At 1 and 10 μM, ATP, dATP, and 3′-dATP were able to efficiently compete with ATPγS for binding to NS4B, unlike the guanine-containing nucleotide triphosphates GTP and dGTP. Furthermore, comparison of adenosine nucleotides ATP, ADP, and AMP suggests the triphosphate moiety plays an important role in binding.

The IC_{50} and K_i values for the more potent competitors of [γ-^{35}S]ATP were determined using the same filtration assay (Table 2). The K_i for ATPγS was ~3.5 μM and matched the K_d values obtained for this nonhydrolyzable analogue using equilibrium and kinetic methods. ATP, 3′-dATP, and 2′-dATP were the most potent competitors of ATPγS, with K_i values of 0.5, 0.62, and 0.86 μM, respectively. These results suggest that the binding of NTPs by NS4B does not critically depend on interactions with hydroxyl groups of the ribose ring at the 2′ and 3′ positions (Table 2). Removing the γ-phosphate (ADP) or the γ- and β-phosphates (AMP) increased the K_i by 16- or 60-fold, respectively, compared to ATP. Although GTP is identical to ATP with the exception of the purine C2 and C6 prosthetic groups, the K_i for GTP was approximately 70-fold higher than that of ATP, suggesting that the binding of ATP involves protein interactions with the purine exocyclic groups. Obtaining complete IC_{50} curves was difficult for GDP and GMP because these nucleotides appear to have weak affinity, thus showing the same trend in affinity that was observed with the adenosine nucleotides (affinity for NTP > NDP > NMP) (Table 2). cAMP and cGMP gave K_i values greater than or equal to those of the respective NMP (Table 2).

Hydrolysis of Nucleotide Substrates by NS4B. The hydrolysis of ATP and GTP by WT NS4B was initially monitored using proton NMR. The results revealed a disappearance of the NTP substrates and the appearance of both NDP and NMP. Control reactions without NS4B showed that GTP and ATP were stable during the time course of the experiments. In subsequent experiments, a reversed-phase HPLC assay was used to characterize the hydrolysis of nucleotide substrates and quantitate both the disappearance of substrate and the appearance of products (Figure 5A,C). To further explore the conversion of nucleotide diphosphate to nucleotide monophosphate, NS4B protein was incubated with ADP or GDP. When NS4B was incubated with ADP, both AMP and ATP products were observed (Figure 5B), suggesting an adenylate kinase-type mechanism (EC 2.7.4.3). A kinetic analysis of the initial velocities for formation of ATP and AMP from ADP showed that the velocities of ATP and AMP formation were each approximately half the velocity for the disappearance of ADP, suggesting that two molecules of ADP were converted to ATP + AMP, consistent with the reverse reaction of adenylate kinase (AK). The production of both ATP and AMP from ADP was confirmed by incubating NS4B with [^{3}H]ADP labeled with tritium at positions 2 and 8 of the adenosine ring. The reaction products, [^{3}H]ATP and [^{3}H]AMP, were detected using an analytical HPLC instrument equipped with a radiometric detector (Figure 6). To further characterize the forward AK reaction, NS4B was incubated with ATP alone or with ATP and an equimolar amount of AMP. Incubation

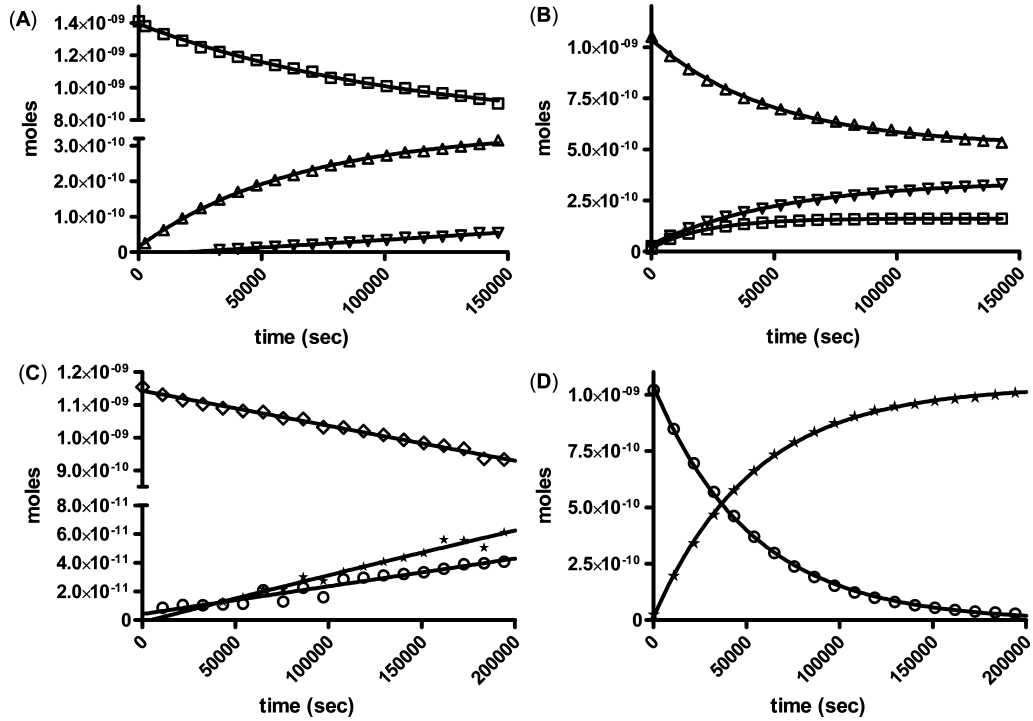

FIGURE 5: Nucleotide hydrolysis time course monitored by HPLC. (A) Incubation of 250 mM ATP (□) with 450 nM NS4B results in the formation of both ADP (△) and AMP (▽). (B) Incubation of 250 mM ADP (△) with 450 nM NS4B results in the formation of AMP (▽) and ATP (□). (C) Incubation of 250 mM GTP (◇) with NS4B results in slow hydrolysis, yielding both GDP (○) and GMP (★). (D) Incubation of 250 mM GDP (○) with NS4B yields only GMP (★). Data were fit to the first-order rate equation to obtain progress curves.

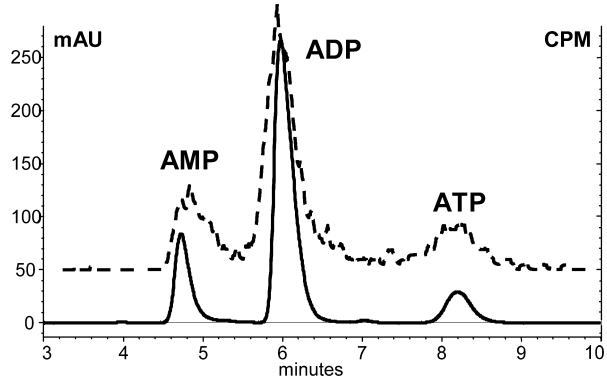

FIGURE 6: Overlay of HPLC absorbance (—) and radiometric detection (---) of ATP and AMP reaction products resulting from incubation of NS4B with ADP substrate (adenylate kinase reaction). Peak retention times coincided with observed peaks from ATP, ADP, and AMP standards. NS4B (450 nM) was incubated with 250 μM [^{3}H]ADP for 1000 min at room temperature.

Table 3: Initial Velocities of NS4B Adenylate Kinase

substrate(s)	velocity (M s^{-1})[a]
250 μM ATP without AMP	1.4×10^{-9}
250 μM ATP and 250 μM AMP	2.8×10^{-9}

[a] Measured as the appearance of the ADP product by reversed-phase HPLC.

of NS4B with AMP in addition to ATP as substrates increased the velocity of ADP production ~2-fold compared to the velocities of reactions with only ATP as a substrate (Table 3).

In contrast to the conversion of ADP into ATP and AMP, incubation of NS4B with GDP yielded a rapid conversion to GMP without the formation of GTP being observed (Figure 5D). The conversion of GTP to GDP and GMP appears to use a mechanism in which the γ- and β-phosphates are sequentially removed from GTP. Analysis of initial velocities of the GTP reaction indicated that hydrolysis of GTP to GDP was the slower rate-limiting step followed by a more rapid conversion of GDP to GMP. Incubation of NS4B with inorganic phosphate and either AMP or GMP did not produce any of the corresponding diphosphates, suggesting that NS4B does not catalyze the addition of inorganic phosphate to NMPs.

The Michaelis−Menten constants, K_m and k_{cat}, were determined by measuring initial velocities when NS4B was incubated with different concentrations of substrates at room temperature (Figure 5A−C of the Supporting Information). The hydrolysis of GDP to GMP occurred at the fastest rate which had a k_{cat} of 31.2×10^{-3} s^{-1}, approximately ~2.5-fold faster than the rate of conversion of ADP to AMP and ATP which had a k_{cat} of 12.5×10^{-3} s^{-1} (Table 4). Consistent with the time course data, the hydrolysis of ATP and GTP to nucleotide diphosphates was relatively slow compared to the conversion of GDP to GMP, suggesting that hydrolysis of the γ-phosphate is rate-limiting. The forward AK reaction was analyzed by holding the ATP concentration constant and varying the concentration of AMP. Plotting s/v versus s indicated the mechanism was either a random ordered ternary complex mechanism or a compulsory ordered ternary complex mechanism (*32*). The reverse AK reaction (2ADP → ATP + AMP) yielded a 1.4-fold larger k_{cat} compared to the forward AK reaction (ATP + AMP → 2ADP) (Table 4), suggesting the reverse AK reaction may be favored *in vivo*.

The intrinsic rate of hydrolysis of GTP by purified human Ras-P21 (GST fusion; Cell Signaling Technologies) was measured using the same HPLC assay and compared to the

Table 4: Kinetic Parameters of Reactions Catalyzed by NS4B

	K_m (M)	k_{cat} (s^{-1})[a]	k_{cat}/K_m ($M^{-1}s^{-1}$)
	WT NS4B		
ATP → ADP	$(99 \pm 7) \times 10^{-6}$	$(4.3 \pm 0.1) \times 10^{-3}$	43.4 ± 3.2
ATP + AMP → 2ADP	$(42 \pm 4) \times 10^{-6}$[b]	$(7.4 \pm 0.1) \times 10^{-3}$	176 ± 17
2ADP → ATP + AMP	$(440 \pm 19) \times 10^{-6}$[c]	$(12.5 \pm 0.3) \times 10^{-3}$	28.4 ± 1.4
GTP → GDP	$(449 \pm 37) \times 10^{-6}$	$(4.5 \pm 0.2) \times 10^{-3}$	10.0 ± 0.9
GDP → GMP	$(466 \pm 12) \times 10^{-6}$	$(31.2 \pm 0.4) \times 10^{-3}$	67 ± 2
	Ras Hydrolysis		
GTP → GDP	$(564 \pm 29) \times 10^{-6}$	$(3.5 \pm 0.1) \times 10^{-3}$	6.2 ± 0.4
	NS4B-KE-DN		
ATP → ADP	$(516 \pm 48) \times 10^{-6}$	$(3.0 \pm 0.1) \times 10^{-3}$	5.8 ± 0.6
2ADP → ATP + AMP	$(591 \pm 38) \times 10^{-6}$[c]	$(14.4 \pm 0.5) \times 10^{-3}$	24.4 ± 1.8
GTP → GDP	$(741 \pm 59) \times 10^{-6}$	$(4.5 \pm 0.2) \times 10^{-3}$	6.1 ± 0.6
GDP → GMP	$(441 \pm 18) \times 10^{-6}$	$(30.2 \pm 0.6) \times 10^{-3}$	68 ± 3
	NS4B-5M		
ATP → ADP	$(763 \pm 78) \times 10^{-6}$	$(4.2 \pm 0.3) \times 10^{-3}$	5.5 ± 0.7
2ADP → ATP + AMP	$\sim 73000 \times 10^{-6}$[c]		
GTP → GDP	$(655 \pm 297) \times 10^{-6}$	$(4.2 \pm 0.1) \times 10^{-3}$	6.4 ± 2.9
GDP → GMP	$(506 \pm 11) \times 10^{-6}$	$(38.5 \pm 0.4) \times 10^{-3}$	76 ± 2

[a] The active enzyme concentration (E_0) was 450 nM (determined as described in Experimental Procedures). [b] Apparent K_m for ATP (bi-bi ternary complex mechanism). [c] Apparent K_m for ADP (bi-bi ternary complex mechanism).

rate of hydrolysis of GTP by NS4B. The k_{cat} for the conversion of GTP to GDP by human Ras-p21 was very similar to the k_{cat} observed with NS4B (Table 4).

Hydrolysis of Nucleotide Substrates by Mutant NS4B. The hydrolyses of ATP and GTP by the double mutant (NS4B-2M) and quintuple mutant (NS4B-5M) NS4B proteins were also characterized using the HPLC assay. These data show that the double mutations of K135E in motif A and D228N in motif B increased the K_m for ATP 5-fold and the K_m for ADP 14-fold but had little effect on the k_{cat} for the hydrolysis of ATP or the conversion of ADP to AMP and ATP (Table 4). In contrast, introduction of the K135E and D228N mutations increased the K_m for GTP 1.7-fold but had little effect on either the K_m or k_{cat} values for the conversion of GDP to GMP (Table 4). Mutation of three additional amino acids in the NS4B-5M mutant resulted in an enzyme with an increased K_m for ATP relative to the double mutant, but with little change in the k_{cat} value for the conversion of ATP to ADP (Table 4). The NS4B-5M mutant exhibited a very low rate of conversion of ADP to ATP and AMP, making measurement of the kinetic parameters difficult. NS4B-5M was able to catalyze the conversion of GTP to GDP and GDP to GMP with a catalytic efficiency that was 30−35% lower than that of the WT protein (Table 4).

DISCUSSION

Previous *in vitro* studies of NS4B have relied on membrane preparations of NS4B containing green fluorescent protein (GFP) or glutathione *S*-transferase (GST) domains attached to either the N- or C-terminus of NS4B (*22*). Our study provides the first quantitative biochemical insight into the enzymatic activities of purified HCV NS4B protein. SDS−PAGE, Western immunoblots, and LC−MS indicated that NS4B was the predominant protein species in the purified preparations with a mass of 29 kDa, matching the expected mass of the recombinant protein. Circular dichroism revealed a well-ordered NS4B protein, suggesting that protein secondary structure is maintained in the detergent-containing buffer used during protein extraction. Mass spectrometry indicated the excision of a methionine and a single acetylation modification, which are both known to occur at the N-terminus of most eukaryotic proteins (*33*−*35*). Mass spectrometry also indicated that NS4B expressed in *Sf9* insect cells is not palmitoylated at the C-terminus, a post-translational modification that has been reported to occur in Huh7 cells (*12*), suggesting that mammalian enzymes are required for palmitoylation.

NTPγAA UV cross-linking studies demonstrated that both ATPγAA and GTPγAA bound to purified NS4B with comparable affinity. This result is in contrast to previous studies in which only GTPγAA was bound by a NS4B−GFP fusion protein in cellular membrane preparations (*22*). Competition of the photoreactive NTP analogues with ATPγS or GTPγS resulted in dose-dependent decreases in the photoaffinity labeling, indicating that the labeling occurred at the same site which binds ATP and GTP. In addition, purified NS4B was not labeled with [α-^{32}P]8N_3-ATP, an analogue that energetically favors the *syn*-conformation due to the presence of an azide moiety at the purine ring C8 position. This suggests that NS4B binds ATP in the *anti*-conformation and further demonstrates the specificity of the labeling. In addition, only the 29 kDa band was labeled with ATPγAA and GTPγAA molecules, indicating that the NS4B protein is responsible for the binding and enzymatic data presented in this report.

Determination of the equilibrium and kinetic disassociation constants (K_d) for ATPγS and GTPγS indicated that NS4B displays a higher affinity for ATPγS. In the presence of Mg^{2+}, ATPγS bound with ~10-fold greater affinity over GTPγS when utilizing the saturation−equilibration method and with ~3-fold greater affinity when using a kinetic approach. Competition binding studies in which nucleotides displaced ATPγS and GTPγS indicated the following hierarchy of binding affinities: NTP > NDP > NMP ≥ cNMP (with higher affinity displayed for adenosine nucleotides compared to guanosine nucleotides). The binding affinity for CTP, UTP, dCTP, and dTTP was lower than the affinity for GTP (K_i = 35.8 μM), indicating specificity for

purine over pyrimidine nucleotides. In addition, NS4B exhibited similar affinities for ATP, dATP, and 3′-dATP, suggesting little specificity for ribose versus deoxyribose sugars.

When nucleotide triphosphate hydrolysis was assessed by proton NMR or reversed-phase HPLC, several interesting enzymatic properties of NS4B were revealed. During the hydrolysis of ATP and GTP, the product nucleotide diphosphate appeared first followed by the appearance of nucleotide monophosphate, suggesting a sequential hydrolysis. Comparisons of initial velocities show that hydrolysis of ATP to ADP was 25-fold faster than the conversion of GTP to GDP. Incubation of NS4B with ADP resulted in the appearance of both ATP and AMP, suggesting adenylate kinase (AK) activity similar to that reported for yeast AK (*36, 37*). To confirm this reaction, NS4B was incubated with [2,8-^{3}H]ADP in the presence of Mg^{2+}, and the appearance of both [^{3}H]ATP and [^{3}H]AMP occurred, suggesting a transfer of the β-phosphate from one ADP to a second ADP molecule. In addition, binding of [^{3}H]ADP to NS4B in the presence of Mg^{2+} yielded a Hill coefficient of 1.73, suggesting that two molecules of ADP were bound (data not shown). Taken together, these results suggest a protein fold (active site) similar to that of AK where ATP or ADP is bound at an ATP site by P-loop amino acids (Walker motif A) and an AMP or ADP molecule is bound at a topologically adjacent AMP site (*38*−*41*). The AMP binding site of AKs consists of hydrophobic amino acids and arginine residues; however, these sites lack conserved motifs and cannot be predicted from the protein primary sequence. Crystallographic studies of AK from *Mycobacterium tuberculosis* have yielded a structure with two ADPs bound (*39*) where a single Mg^{2+} atom forms hydrogen bonds with both the protein and the β-phosphates of each ADP to facilitate transfer of the phosphate group. While most AKs, including the small bacterial AK, favor the forward reaction ATP + AMP → 2ADP, these reactions are almost isoenergetic, and thus, these enzymes can also catalyze the reverse reaction 2ADP → ATP + AMP. Baker's yeast AK and NS4B appear to favor this reverse reaction but are capable of catalyzing the forward reaction at a slower rate. In the absence of AMP, NS4B appears to bind ATP and produces ADP and P_i; however, the efficiency of this reaction is much lower compared to that of the conversion of 2ADP to ATP and AMP. In contrast to the reaction observed with ADP, the incubation of NS4B with GDP produces only GMP. This result suggests that the putative AMP binding site of NS4B is specific for ADP or AMP but has a very low affinity for GDP or GMP. This substrate specificity has been observed in various AKs and is due to the formation of numerous hydrogen bonds between the protein and the base pairing face of the nucleotide (*39, 42, 43*).

To confirm that the ATPγS and GTPγS binding, ATP and GTP hydrolysis, and AK activity were associated with the recombinant NS4B protein, amino acid substitutions were introduced into Walker motifs A, B, and G. These motifs are involved in the binding of the α-phosphate (PM1), the γ-phosphate (PM3), and the purine ring (G) for NTP substrates. Structural data for *M. tuberculosis* AK indicate the Walker motif A (P-loop) is involved in binding of ATP in the AK active site (*39*). The double mutant NS4B-2M was able to bind both ATPγS and GTPγS, although with significantly lower affinity, whereas the quintuple mutant NS4B-5M was essentially unable to bind either ATPγS or GTPγS. These mutation data are supportive of previous binding studies involving GTPγS (*44*). Measurement of enzymatic constants for the NS4B-2M mutant demonstrated a 5-fold increase in the K_m for ATP and a 14-fold increase in the K_m for ADP substrates with little change in the k_{cat}, suggesting that these mutations had a strong effect on binding of ATP and ADP but little or no effect on the turnover rate. Additional mutations in the P-loop (motif A) and the G motif resulted in even weaker binding of ATP and ADP to NS4B, and extremely low turnover rates, making accurate measurements of K_m and k_{cat} difficult. Notably, while these mutations in the Walker motifs had a dramatic effect on GTPγS binding, these mutations gave only minimal increases in the K_m for GTP and the K_m for GDP when hydrolysis of these substrates was assessed. The results from mutant NS4B protein preparations indicate the ATPγS and GTPγS binding, ATP and GTP hydrolysis, and AK activities are associated with NS4B and are not due to a contaminating host cell protein.

The potential roles of NS4B GTP and GDP hydrolysis and adenylate kinase activity in the HCV-infected hepatocyte remain unclear. Evidence that RNA viruses recruit small cellular GTPases for various viral activities is emerging. HCV NS4B has been shown to interact with Rab5, a member of the Ras superfamily involved in the regulation of membrane fusion (*45*), and activation of the N-Ras-PI3K-Akt pathway has been reported in Huh7 cells expressing HCV replicon (*46*). More recent studies have shown that NS4B possesses the ability to transform cells, suggesting this protein may function as an oncogene similar to Ras (*44*). The small GTPases have slow intrinsic rates of GTP hydrolysis in the absence of their corresponding GTPase activating proteins (GAPs) (*47, 48*), and in the reversed-phase HPLC assay, the rate of hydrolysis of GTP by NS4B was very similar to the intrinsic rate of GTP hydrolysis by recombinant Ras-p21 ($k_{cat} = 4.5 \times 10^{-3}$ s^{-1} for NS4B vs $k_{cat} = 3.5 \times 10^{-3}$ s^{-1} for Ras-p21; see Table 4). It is possible that the slow hydrolysis of GTP to GDP catalyzed by NS4B represents intrinsic GTPase activity in the absence of an activating protein, although no specific activating protein for HCV NS4B has yet been discovered.

It is known that replication of all positive-stranded RNA viruses studied to date occurs in association with membranous structures derived from remodeled membranes of various intracellular origins (*49, 50*). In the well-studied Picornaviridae family of viruses, including poliovirus (PV), the nonstructural 2C protein is believed to play a significant role in the reorganization of intracellular membranes to generate vesicle clusters on which viral RNA replication occurs. When the PV 2C protein is expressed alone, the protein localizes to the ER, resulting in the expansion of this organelle into vesicles 50−350 nm in diameter and tubular structures (*51, 52*). Interestingly, the 2C protein sequence contains Walker motifs A and B, and the 2C protein is able to hydrolyze GTP, dATP, and ATP, showing a preference for ATP ($K_m = 700\ \mu$M) (*53, 54*). The function of poliovirus 2C NTPase activity is not understood; however, mutations in the nucleotide binding motif of 2C severely impair viral replication (*53*), similar to the results obtained when Walker motifs A, B, and G are mutated in HCV NS4B (*22, 44*). In addition to poliovirus 2C, the catalytic properties of the 2C

protein from picornaviral human parechovirus 1 have recently been reported (*55*), and the activity of this enzyme shows similarities to the enzymatic properties of HCV NS4B. The parechovirus 2C enzyme was able to sequentially hydrolyze ATP to ADP and AMP with K_m values in the low micromolar range (ATP $K_m = 3.4 \pm 1.6$ μM; ADP $K_m = 0.65 \pm 0.20$ μM) (*55*). The parechovirus 2C protein also catalyzed the conversion of AMP and ATP to 2ADP (AMP kinase/adenylate kinase activity) (*55*). It appears, therefore, that HCV NS4B displays enzymatic activity very similar to those of the picornaviral 2C proteins and functions in a manner similar to that of picornaviral 2C proteins with regard to the reorganization of cellular membranes.

Although the function of NS4B in the replication complex is far from being fully understood, it is clear that the nucleotide binding motif is critical for HCV replication (*22, 44*). The detection of adenylate kinase and GDP hydrolysis activities in purified preparations of NS4B, together with confirmation of previously described GTPase activity, sheds light on the enzymatic activity of this nonstructural protein. Additional studies, however, are needed to fully understand the roles these enzymatic activities play during replication of HCV in infected hepatocytes.

ACKNOWLEDGMENT

We thank Terri Quenzer for performing the limited tryptic digestion and MS/MS amino acid sequencing and Stephan Grant for critical review of the manuscript.

SUPPORTING INFORMATION AVAILABLE

Additional figures showing Western immunoblots, LC−MS, circular dichroism, purity of WT and mutant NS4B preparations by SDS−PAGE, progress curves of ATPγS and GTPγS binding, graph of nucleotide competition for ATPγS/Mg^{2+} binding, and example K_m curves of nucleotide hydrolysis. This material is available free of charge via the Internet at http://pubs.acs.org.

REFERENCES

1. Bartenschlager, R., Frese, M., and Pietschmann, T. (2004) Novel insights into hepatitis C virus replication and persistence. *Adv. Virus Res. 63*, 71–180.
2. Egger, D., Wolk, B., Gosert, R., Bianchi, L., Blum, H. E., Moradpour, D., and Bienz, K. (2002) Expression of hepatitis C virus proteins induces distinct membrane alterations including a candidate viral replication complex. *J. Virol. 76*, 5974–5984.
3. El-Hage, N., and Luo, G. (2003) Replication of hepatitis C virus RNA occurs in a membrane-bound replication complex containing nonstructural viral proteins and RNA. *J. Gen. Virol. 84*, 2761–2769.
4. Gosert, R., Egger, D., Lohmann, V., Bartenschlager, R., Blum, H. E., Bienz, K., and Moradpour, D. (2003) Identification of the hepatitis C virus RNA replication complex in Huh-7 cells harboring subgenomic replicons. *J. Virol. 77*, 5487–5492.
5. Mottola, G., Cardinali, G., Ceccacci, A., Trozzi, C., Bartholomew, L., Torrisi, M. R., Pedrazzini, E., Bonatti, S., and Migliaccio, G. (2002) Hepatitis C virus nonstructural proteins are localized in a modified endoplasmic reticulum of cells expressing viral subgenomic replicons. *Virology 293*, 31–43.
6. Miyanari, Y., Hijikata, M., Yamaji, M., Hosaka, M., Takahashi, H., and Shimotohno, K. (2003) Hepatitis C virus non-structural proteins in the probable membranous compartment function in viral genome replication. *J. Biol. Chem. 278*, 50301–50308.
7. Moradpour, D., Gosert, R., Egger, D., Penin, F., Blum, H. E., and Bienz, K. (2003) Membrane association of hepatitis C virus nonstructural proteins and identification of the membrane alteration that harbors the viral replication complex. *Antiviral Res. 60*, 103–109.
8. Aizaki, H., Lee, K. J., Sung, V. M., Ishiko, H., and Lai, M. M. (2004) Characterization of the hepatitis C virus RNA replication complex associated with lipid rafts. *Virology 324*, 450–461.
9. Quinkert, D., Bartenschlager, R., and Lohmann, V. (2005) Quantitative analysis of the hepatitis C virus replication complex. *J. Virol. 79*, 13594–13605.
10. Yang, G., Pevear, D. C., Collett, M. S., Chunduru, S., Young, D. C., Benetatos, C., and Jordan, R. (2004) Newly synthesized hepatitis C virus replicon RNA is protected from nuclease activity by a protease-sensitive factor(s). *J. Virol. 78*, 10202–10205.
11. Lundin, M., Monne, M., Widell, A., Von Heijne, G., and Persson, M. A. (2003) Topology of the membrane-associated hepatitis C virus protein NS4B. *J. Virol. 77*, 5428–5438.
12. Yu, G. Y., Lee, K. J., Gao, L., and Lai, M. M. (2006) Palmitoylation and polymerization of hepatitis C virus NS4B protein. *J. Virol. 80*, 6013–6023.
13. Lundin, M., Lindstrom, H., Gronwall, C., and Persson, M. A. (2006) Dual topology of the processed hepatitis C virus protein NS4B is influenced by the NS5A protein. *J. Gen. Virol. 87*, 3263–3272.
14. Elazar, M., Liu, P., Rice, C. M., and Glenn, J. S. (2004) An N-terminal amphipathic helix in hepatitis C virus (HCV) NS4B mediates membrane association, correct localization of replication complex proteins, and HCV RNA replication. *J. Virol. 78*, 11393–11400.
15. Welsch, C., Albrecht, M., Maydt, J., Herrmann, E., Welker, M. W., Sarrazin, C., Scheidig, A., Lengauer, T., and Zeuzem, S. (2007) Structural and functional comparison of the non-structural protein 4B in flaviviridae. *J. Mol. Graphics Modell. 26*, 546–557.
16. Dimitrova, M., Imbert, I., Kieny, M. P., and Schuster, C. (2003) Protein-protein interactions between hepatitis C virus nonstructural proteins. *J. Virol. 77*, 5401–5414.
17. Ishido, S., Fujita, T., and Hotta, H. (1998) Complex formation of NS5B with NS3 and NS4A proteins of hepatitis C virus. *Biochem. Biophys. Res. Commun. 244*, 35–40.
18. Piccininni, S., Varaklioti, A., Nardelli, M., Dave, B., Raney, K. D., and McCarthy, J. E. (2002) Modulation of the hepatitis C virus RNA-dependent RNA polymerase activity by the non-structural (NS) 3 helicase and the NS4B membrane protein. *J. Biol. Chem. 277*, 45670–45679.
19. Blight, K. J. (2007) Allelic variation in the hepatitis C virus NS4B protein dramatically influences RNA replication. *J. Virol. 81*, 5724–5736.
20. Grassmann, C. W., Isken, O., Tautz, N., and Behrens, S. E. (2001) Genetic analysis of the pestivirus nonstructural coding region: Defects in the NS5A unit can be complemented in trans. *J. Virol. 75*, 7791–7802.
21. Khromykh, A. A., Sedlak, P. L., and Westaway, E. G. (2000) cis- and trans-acting elements in flavivirus RNA replication. *J. Virol. 74*, 3253–3263.
22. Einav, S., Elazar, M., Danieli, T., and Glenn, J. S. (2004) A nucleotide binding motif in hepatitis C virus (HCV) NS4B mediates HCV RNA replication. *J. Virol. 78*, 11288–11295.
23. Delvecchio, A. Z., and Weidong (1999) Screening Methods Using as ATPase Protein from a Virus of the Flaviviridae Family. WO 99/01582.
24. Delvecchio, A. Z., and Weidong (Smithkline Beecham Corp.) (2000) Screening Methods using an ATPase protein from Hepatitis C virus. U.S. Patent 6010848.
25. Guo, J. T., Bichko, V. V., and Seeger, C. (2001) Effect of α-interferon on the hepatitis C virus replicon. *J. Virol. 75*, 8516–8523.
26. Lohmann, V., Hoffmann, S., Herian, U., Penin, F., and Bartenschlager, R. (2003) Viral and cellular determinants of hepatitis C virus RNA replication in cell culture. *J. Virol. 77*, 3007–3019.
27. Cheng, Y., and Prusoff, W. H. (1973) Relationship between the inhibition constant (K1) and the concentration of inhibitor which causes 50% inhibition (I50) of an enzymatic reaction. *Biochem. Pharmacol. 22*, 3099–3108.
28. Grubbs, R. D. (2002) Intracellular magnesium and magnesium buffering. *BioMetals 15*, 251–259.
29. Ash, D. E., and Schramm, V. L. (1982) Determination of free and bound manganese(II) in hepatocytes from fed and fasted rats. *J. Biol. Chem. 257*, 9261–9264.
30. Barbacid, M. (1987) ras genes. *Annu. Rev. Biochem. 56*, 779–827.

31. Valencia, A., Chardin, P., Wittinghofer, A., and Sander, C. (1991) The ras protein family: Evolutionary tree and role of conserved amino acids. *Biochemistry 30*, 4637–4648.
32. Cornish-Bowden, A. (1995) *Fundamentals of Enzyme Kinetics*, Portland Press Ltd., London.
33. Bradshaw, R. A., Brickey, W. W., and Walker, K. W. (1998) N-Terminal processing: The methionine aminopeptidase and Nα-acetyl transferase families. *Trends Biochem. Sci. 23*, 263–267.
34. Polevoda, B., and Sherman, F. (2003) Composition and function of the eukaryotic N-terminal acetyltransferase subunits. *Biochem. Biophys. Res. Commun. 308*, 1–11.
35. Polevoda, B., and Sherman, F. (2003) N-Terminal acetyltransferases and sequence requirements for N-terminal acetylation of eukaryotic proteins. *J. Mol. Biol. 325*, 595–622.
36. Sheng, X. R., Li, X., and Pan, X. M. (1999) An iso-random Bi Bi mechanism for adenylate kinase. *J. Biol. Chem. 274*, 22238–22242.
37. Su, S., and Russell, P. J., Jr. (1968) Adenylate kinase from bakers' yeast. 3. Equilibria: equilibrium exchange and mechanism. *J. Biol. Chem. 243*, 38263833.
38. Abele, U., and Schulz, G. E. (1995) High-resolution structures of adenylate kinase from yeast ligated with inhibitor Ap5A, showing the pathway of phosphoryl transfer. *Protein Sci. 4*, 1262–1271.
39. Bellinzoni, M., Haouz, A., Grana, M., Munier-Lehmann, H., Shepard, W., and Alzari, P. M. (2006) The crystal structure of *Mycobacterium tuberculosis* adenylate kinase in complex with two molecules of ADP and Mg^{2+} supports an associative mechanism for phosphoryl transfer. *Protein Sci. 15*, 1489–1493.
40. Berry, M. B., Bae, E., Bilderback, T. R., Glaser, M., and Phillips, G. N., Jr. (2006) Crystal structure of ADP/AMP complex of *Escherichia coli* adenylate kinase. *Proteins 62*, 555–556.
41. Berry, M. B., and Phillips, G. N., Jr. (1998) Crystal structures of *Bacillus stearothermophilus* adenylate kinase with bound Ap5A, Mg^{2+} Ap5A, and Mn^{2+} Ap5A reveal an intermediate lid position and six coordinate octahedral geometry for bound Mg^{2+} and Mn^{2+}. *Proteins 32*, 276–288.
42. Krishnamurthy, H., Lou, H., Kimple, A., Vieille, C., and Cukier, R. I. (2005) Associative mechanism for phosphoryl transfer: A molecular dynamics simulation of *Escherichia coli* adenylate kinase complexed with its substrates. *Proteins 58*, 88–100.
43. Willemoes, M., and Kilstrup, M. (2005) Nucleoside triphosphate synthesis catalysed by adenylate kinase is ADP dependent. *Arch. Biochem. Biophys. 444*, 195–199.
44. Einav, S., Sklan, E. H., Moon, H. M., Gehrig, E., Liu, P., Hao, Y., Lowe, A. W., and Glenn, J. S. (2008) The nucleotide binding motif of hepatitis C virus NS4B can mediate cellular transformation and tumor formation without Ha-ras co-transfection. *Hepatology 47*, 827–835.
45. Stone, M., Jia, S., Heo, W. D., Meyer, T., and Konan, K. V. (2007) Participation of rab5, an early endosome protein, in hepatitis C virus RNA replication machinery. *J. Virol. 81*, 4551–4563.
46. Mannova, P., and Beretta, L. (2005) Activation of the N-Ras-PI3K-Akt-mTOR pathway by hepatitis C virus: Control of cell survival and viral replication. *J. Virol. 79*, 8742–8749.
47. Bernards, A. (2003) GAPs galore! A survey of putative Ras superfamily GTPase activating proteins in man and *Drosophila*. *Biochim. Biophys. Acta 1603*, 47–82.
48. Scheffzek, K., and Ahmadian, M. R. (2005) GTPase activating proteins: Structural and functional insights 18 years after discovery. *Cell. Mol. Life Sci. 62*, 3014–3038.
49. Belov, G. A., Altan-Bonnet, N., Kovtunovych, G., Jackson, C. L., Lippincott-Schwartz, J., and Ehrenfeld, E. (2007) Hijacking components of the cellular secretory pathway for replication of poliovirus RNA. *J. Virol. 81*, 558–567.
50. Salonen, A., Ahola, T., and Kaariainen, L. (2005) Viral RNA replication in association with cellular membranes. *Curr. Top. Microbiol. Immunol. 285*, 139–173.
51. Cho, M. W., Teterina, N., Egger, D., Bienz, K., and Ehrenfeld, E. (1994) Membrane rearrangement and vesicle induction by recombinant poliovirus 2C and 2BC in human cells. *Virology 202*, 129–145.
52. Teterina, N. L., Gorbalenya, A. E., Egger, D., Bienz, K., and Ehrenfeld, E. (1997) Poliovirus 2C protein determinants of membrane binding and rearrangements in mammalian cells. *J. Virol. 71*, 8962–8972.
53. Pfister, T., and Wimmer, E. (1999) Characterization of the nucleoside triphosphatase activity of poliovirus protein 2C reveals a mechanism by which guanidine inhibits poliovirus replication. *J. Biol. Chem. 274*, 6992–7001.
54. Rodriguez, P. L., and Carrasco, L. (1993) Poliovirus protein 2C has ATPase and GTPase activities. *J. Biol. Chem. 268*, 8105–8110.
55. Samuilova, O., Krogerus, C., Fabrichniy, I., and Hyypia, T. (2006) ATP hydrolysis and AMP kinase activities of nonstructural protein 2C of human parechovirus 1. *J. Virol. 80*, 1053–1058.

BI801747P